SUPPLEMENTARY INFORMATION: The Role of Surface Stoichiometry in NO_2 Gas Sensing Using Single and Multiple Nanobelts of Tin Oxide

Mateus G. Masteghin [a,b], Ranilson A. Silva [b], David C. Cox [a], Denis R. M. Godoi [b], S. Ravi P. Silva [a,], Marcelo O. Orlandi [b,*]*

[a] Advanced Technology Institute, University of Surrey, Guildford, GU2 7XH, UK.

[b] Department of Physical-Chemistry, São Paulo State University, Araraquara, 14800-900, Brazil.

[*]corresponding authors: s.silva@surrey.ac.uk (S.R.P. Silva), and marcelo.orlandi@unesp.br (M.O. Orlandi).

METHODS

Carbothermal reduction synthesis

The starting material was a 1g mixture of SnO_2 powder (Sigma-Aldrich, São Paulo, Brazil, 99.9% purity) and carbon black (Union Carbide, São Paulo, Brazil, >99% purity) in the molar ratio of 1.5:1. The crucible containing the initial mixture was inserted into the center of the tube furnace which was heated to 1135 °C using a heating rate of 10 °C min^{-1}. The furnace was then held at that temperature for 75 min. In order to obtain the reduced SnO nanobelts, a constant flux of N_2 (150 cm^3 min^{-1}) was used; and, to obtain the Sn_3O_4 and SnO_2, a constant flux of N_2 (160 cm^3 min^{-1}) was upheld during the entire synthesis together with an oxygen counter flow (0.6 cm^3 min^{-1}) starting when the temperature reached 900 °C. At the end of the synthesis, the materials were retrieved from inside the alumina tube. The SnO nanobelts formed during the synthesis under reducing atmosphere were separated from the SnO micro-disks by a decantation process, and the Sn_3O_4 and SnO_2 formed in a mixed atmosphere were separated by their color and final position. The Sn_3O_4 presents itself as a yellowish material which has been formed closer to the center of the tube, while the white colored SnO_2 nanobelts were closer to the O_2 gas inlet. In addition, a greyish SnO_2 was also formed and was located in a region between the Sn_3O_4 and the white colored SnO_2.

EXTRA RESULTS

Band-gap determination by photocurrent measurements

Photocurrent measurements are a powerful tool to obtain the optical properties of semiconducting materials since it does not require the need to find the intercept of the linear part of the graph with the energy axis (as in the Tauc-plot [1]) once the band-gap is obtained by the mean value of the Gauss fitting on the photocurrent peak. This current peak appears as a result of the stimulation of the electrons lying at the valence band maximum to the conduction band minimum, where the delocalized carriers will be contributing to a conductivity increasing at wavelengths corresponding to the band-gap value.[2]

Comparing Fig. S1a with Fig. S1b, one can see a behaviour difference between the SnO_2 and the Sn_3O_4, respectively, in which the later presented the so-called persistent photoconductance.[3] This effect can be a result of the band bending generated when the material was exposed to the dry air flow - allowing the adsorption/chemisorption of molecules on its surface - and it is highly sensitive to the diameter of the nanowires, which is smaller for the Sn_3O_4.[4,5]

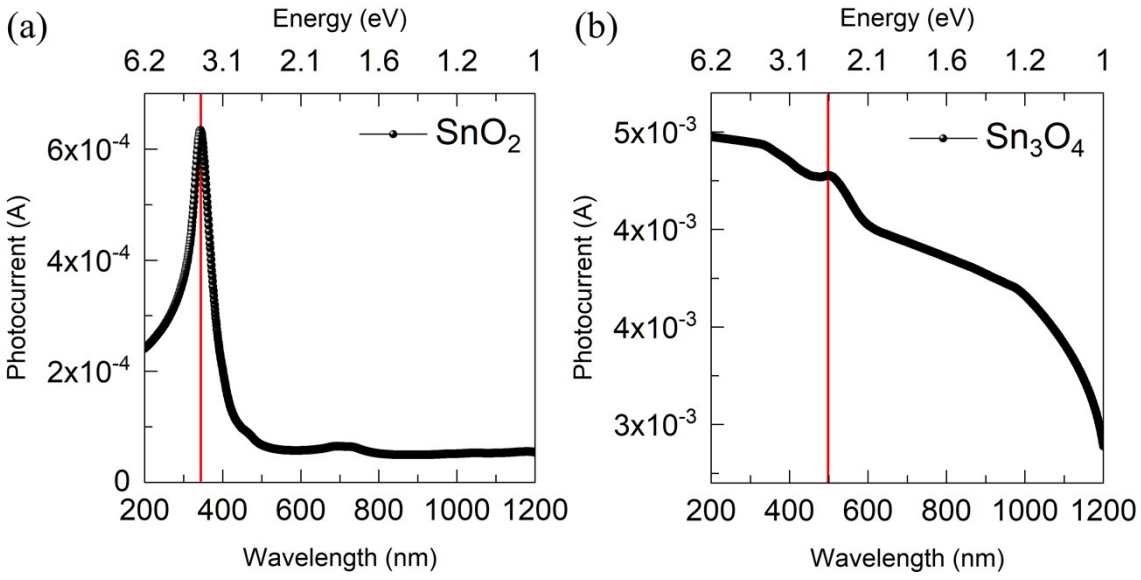

Fig. S1. Photocurrent measurements for the (a) white colored SnO_2 nanobelts, and (b) Sn_3O_4 nanobelts. Optical band-gaps of 3.6 eV and 2.5 eV have been obtained for the SnO_2 and Sn_3O_4, respectively.

Raman measurements of the SnO, and the grey SnO_2 nanobelts

The Raman spectrum of the SnO nanobelts can be seen in Fig. S2. One can see a majority of the SnO phase, indicated by the E_{1g} and A_{1g} vibrational modes at 114 cm^{-1} and 211 cm^{-1}, respectively, and another E_{1g} mode at 450 cm^{-1}.[6–8] The peaks assigned as Sn_3O_4 (two A_g modes at 77 cm^{-1} and 141 cm^{-1}, and two B_g modes at 94 cm^{-1} and 170 cm^{-1}) and Sn_2O_3 (a B_g mode at 160 cm^{-1}) are most probably related to oxygen adsorbed/chemisorbed on the SnO surface.[8–10] It is possible to see the mentioned minor phases on the Raman spectrum because it is affected by both the local bonding and the long-range arrangement.[8] Further characterization (XRD and TEM) of the SnO nanobelts obtained by the carbothermal reduction method can be found in the works of Suman *et al.*[11] and Orlandi *et al.*[12].

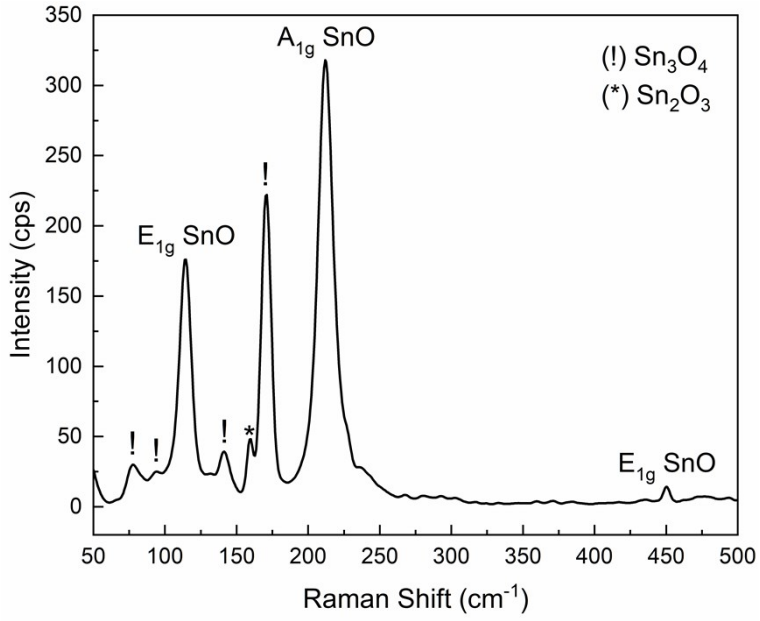

Fig. S2. Raman spectrum for the SnO nanobelts showing a major SnO phase indicated by the A_{1g} and E_{1g} vibrational modes, and minor Sn_3O_4 and Sn_2O_3 clusters indicated by the "!" and "*", respectively.

Looking at Fig. S3 one can observe that in addition to the vibrational modes assigned to the white SnO_2 in Fig. 1a, the grey SnO_2 presents extra peaks corresponding to Sn_3O_4 clusters at 94 cm^{-1} (B_g), 132 cm^{-1} (B_g), and 170 cm^{-1} (B_g); besides Sn_2O_3 clusters at 235 cm^{-1} (A_g), and 542 cm^{-1} (A_g). Liu *et al.* [13] showed that after annealing SnO_2 particles with oxygen flow, the peak attributed here to the Sn_2O_3 A_g mode (235 cm^{-1}) disappears, while the peak at 170 cm^{-1} for the white SnO_2 (B_g mode) shifts to lower Raman shift values.[13] Those differences are

attributed to O_2 vacancies,[13] which is reasonable bearing in mind that the grey SnO_2 was formed in inner regions of the tube with lower amount of O_2 available.

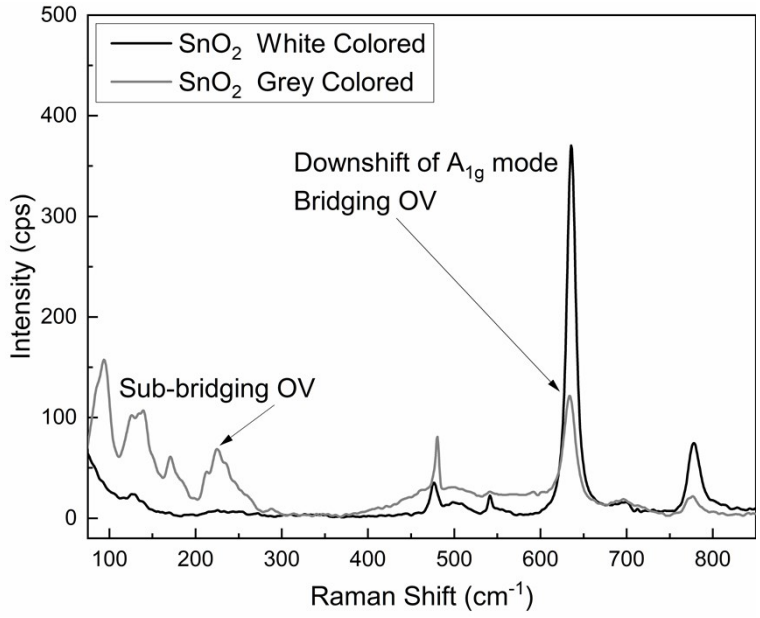

Fig. S3. Raman spectra comparing the white and grey colored SnO_2 nanobelts. The measurement shows that in addition to the expected vibrational modes of the SnO_2, the grey nanobelts present a few peaks attributed to oxygen vacancies.

SnO nanobelt single-devices nanofabrication

Fig. S4 shows 6 devices containing a single-SnO nanobelt. Although the devices look to be well connected to the electrodes, none of them presented a considerable signal to noise ratio regarding the resistance measured before and after the NO_2 release.

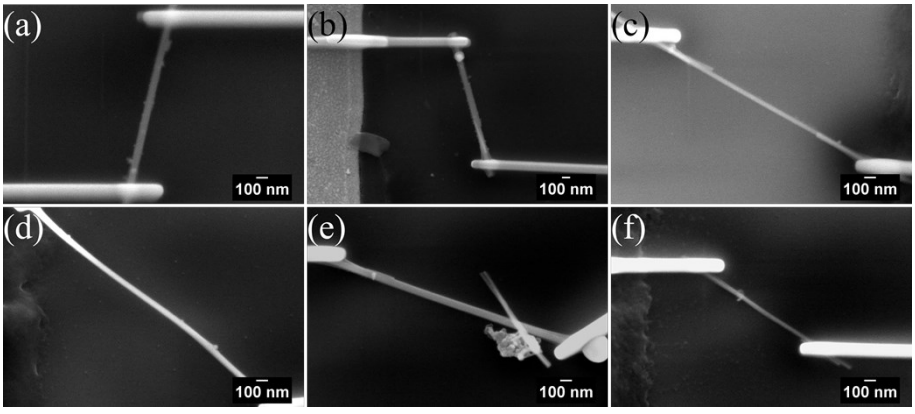

Fig. S4. SEM images of the nanofabricated SnO single-nanobelts. Fig.s a-f correspond to six different nanobelts prepared on distinct electrodes.

XRD of the white and grey colored SnO_2 nanobelts

Fig. S5 presents the XRD pattern for both white and grey coloured SnO_2. Even though the Raman measurements shows a higher amount of oxygen vacancies for the grey SnO_2, the XRD still shows only the *Cassiterite* phase of the SnO_2 (Space group $P4_2/mnm$, *Rutile*-type Tetragonal structure, PDF #41-1445).[14,15] This supports the evidence of having oxygen vacancies mainly on the surface, once differently from the Raman technique, the XRD is concerned with the long-range 3D arrangement of atoms.[8]

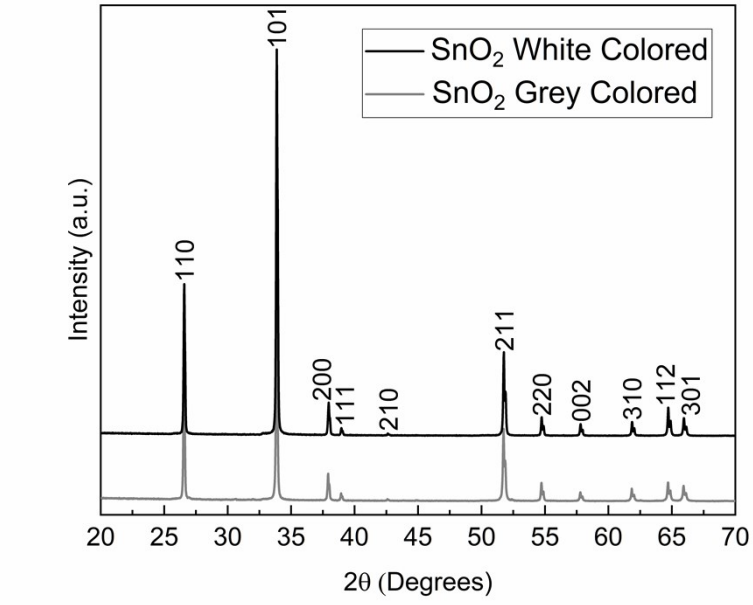

Fig. S5. X-ray diffraction pattern (XRD) of the white and grey SnO_2 nanobelts. Both of them presents only the *Cassiterite* phase wherein the planes were indexed.

Self-heated gas sensor measurements using multi-element devices: sensor signal versus temperature.

During this study, gas sensor measurements were carried out at 150 °C, 200 °C, 250 °C, and 300 °C, all of which used a constant flow of 200 cm^3 min^{-1} and similar NO_2 concentrations. Figure S6 presents the sensor signals obtained under 100 ppm NO_2 exposure, showing best response (highest sensor signal) at 150 °C.

Typically, semiconducting metal oxides (SMOs) require relatively high operating temperatures due to the fact that slow kinetics prevents a decent signal-to-noise ratio at room temperature, being the limiting step the charge transfer from the SMO surface to the chemisorbed molecule. On the other hand, temperatures too elevated cause enhanced desorption and no charge transfer occurs at the interface.[16] Besides, carrying on the

measurements at temperatures above 150 ^{o}C prevents a thin layer of adsorbed water molecules to cover the SMO surface in case humidity is present, allowing a direct measurement of the sensor signal to NO_2 molecules without any cross-sensitivy.[17]

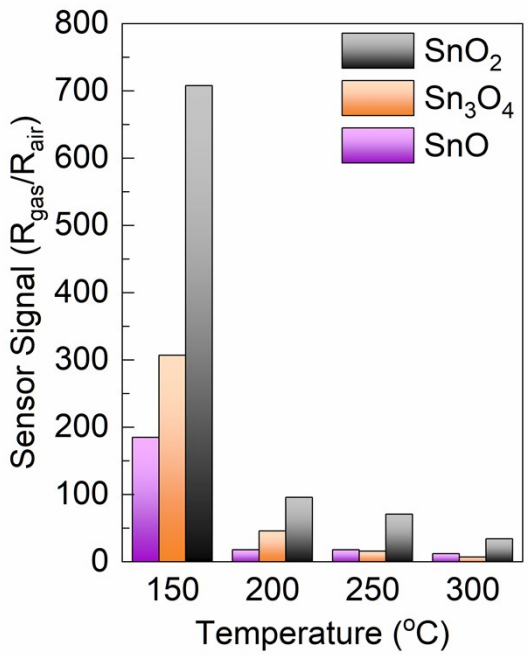

Fig. S6. Multi-device ("carpet" mode) sensor signals as a function of temperature for 100 ppm of NO_2. The temperatures were reached via self-heated electrodes.

Self-heated gas sensor measurements using multi-element devices: grey colored SnO_2 nanobelts.

Finally, Fig. S7 shows the gas sensor measurements using the multi-devices mode. The difference between Fig. S7 and Fig. 6 is that the grey SnO_2 nanobelts is included here. Fig. S7 is used to support the sensor signal trend based on the stoichiometric and reduced surfaces of the Sn-O system, as discussed in the main manuscript.

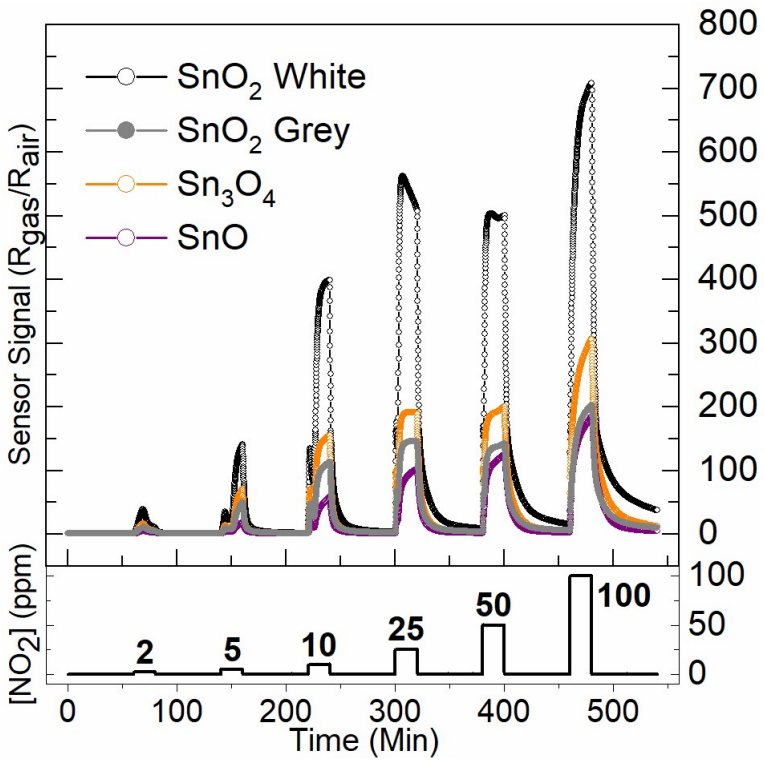

Fig. S7. Multi-devices ("carpet" mode) gas sensor measurements showed as sensor signal *versus* analyte gas concentrations ([NO_2] from 2 to 100 ppm). Black circles correspond to the white colored SnO_2, orange circles to the Sn_3O_4, and purple to the SnO nanobelts. In addition to Fig. 6 of the main manuscript, the grey circles show gas sensor signals for the grey coloured SnO_2. Sensor signals for the grey SnO_2 can be found between the SnO and the Sn_3O_4 NBs. The temperature was kept at 150 °C by self-heated electrodes.

REFERENCES

1 A. Sáenz-Trevizo, P. Amézaga-Madrid, P. Pizá-Ruiz, W. Antúnez-Flores and M. Miki-Yoshida, *Mater. Res.*, 2016, **19**, 33–38.

2 R. López and R. Gómez, *J. sol-gel Sci. Technol.*, 2012, **61**, 1–7.

3 E. Arslan, S. Bütün, S. B. Lisesivdin, M. Kasap, S. Ozcelik and E. Ozbay, *J. Appl. Phys.*, 2008, **103**, 103701.

4 J. D. Prades, F. Hernandez-Ramirez, R. Jimenez-Diaz, M. Manzanares, T. Andreu, A. Cirera, A. Romano-Rodriguez and J. R. Morante, *Nanotechnology*, 2008, **19**, 465501.

5 R. Calarco, M. Marso, T. Richter, A. I. Aykanat, R. Meijers, A. vd Hart, T. Stoica and H. Lüth, *Nano Lett.*, 2005, **5**, 981–984.

6 Y. W. Li, Y. Li, T. Cui, L. J. Zhang, Y. M. Ma and G. T. Zou, *J. Phys. Condens. Matter*, 2007, **19**, 425230.

7 X. Wang, F. X. Zhang, I. Loa, K. Syassen, M. Hanfland and Y. Mathis, *Phys. status solidi*, 2004, **241**, 3168–3178.

8 B. Eifert, M. Becker, C. T. Reindl, M. Giar, L. Zheng, A. Polity, Y. He, C. Heiliger and P. J. Klar, *Phys. Rev. Mater.*, 2017, **1**, 14602.

9 F. Wang, X. Zhou, J. Zhou, T.-K. Sham and Z. Ding, *J. Phys. Chem. C*, 2007, **111**, 18839–18843.

10 O. M. Berengue, R. A. Simon, A. J. Chiquito, C. J. Dalmaschio, E. R. Leite, H. A. Guerreiro and F. E. G. Guimarães, *J. Appl. Phys.*, 2010, **107**, 33717.

11 P. H. Suman, A. A. Felix, H. L. Tuller, J. A. Varela and M. O. Orlandi, *Sensors Actuators B Chem.*, 2015, **208**, 122–127.

12 M. O. Orlandi, P. H. Suman, R. A. Silva and E. P. S. Arlindo, in *Recent Advances in Complex Functional Materials*, Springer, 2017, pp. 43–67.

13 L. Z. Liu, T. H. Li, X. L. Wu, J. C. Shen and P. K. Chu, *J. Raman Spectrosc.*, 2012, **43**, 1423–1426.

14 G. J. McCarthy and J. M. Welton, *Powder Diffr.*, 1989, **4**, 156–159.

15 Z. M. Jarzebski and J. P. Marton, *J. Electrochem. Soc.*, 1976, **123**, 199C-205C.

16 C. Wang, L. Yin, L. Zhang, D. Xiang and R. Gao, *Sensors*, 2010, **10**, 2088–2106.

17 A. Helwig, G. Müller, G. Sberveglieri and M. Eickhoff, *J. Sensors*.